European Journal of Nuclear Medicine and Molecular Imaging

Individual-level metabolic connectivity from dynamic [^{18}F]FDG PET reveals glioma-induced impairments in brain architecture and offers novel insights beyond the SUVR clinical standard

Giulia Vallini, Erica Silvestri†, Tommaso Volpi†, John J. Lee, Andrei G. Vlassenko, Manu S. Goyal, Diego Cecchin, Maurizio Corbetta and Alessandra Bertoldo

†**These authors contributed equally to this work.**

Author information

Corresponding author: Alessandra Bertoldo
Department of Information Engineering, University of Padova, Padova, Italy
Padova Neuroscience Center, University of Padova, Padova, Italy
E-mail: bertoldo@dei.unipd.it
https://orcid.org/0000-0002-6262-6354

Giulia Vallini
Department of Information Engineering, University of Padova, Padova, Italy
giulia.vallini@phd.unipd.it
https://orcid.org/0000-0002-9634-8401

Erica Silvestri
Department of Information Engineering, University of Padova, Padova, Italy
https://orcid.org/0000-0002-1853-0777

Tommaso Volpi
Padova Neuroscience Center, University of Padova, Padova, Italy
Department of Radiology and Biomedical Imaging, Yale University, New Haven, CT, USA
https://orcid.org/0000-0002-5451-6710

John J. Lee
Neuroimaging Laboratories at the Mallinckrodt Institute of Radiology, Washington University School of Medicine, St Louis, MO, USA
https://orcid.org/0000-0003-2269-6267

Andrei G. Vlassenko
Neuroimaging Laboratories at the Mallinckrodt Institute of Radiology, Washington University School of Medicine, St Louis, MO, USA

Manu S. Goyal
Neuroimaging Laboratories at the Mallinckrodt Institute of Radiology, Washington University School of Medicine, St Louis, MO, USA
https://orcid.org/0000-0003-1970-4270

Diego Cecchin
Padova Neuroscience Center, University of Padova, Padova, Italy
Department of Medicine, Unit of Nuclear Medicine, University of Padova, Padova, Italy
https://orcid.org/0000-0001-7956-1924

Maurizio Corbetta
Padova Neuroscience Center, University of Padova, Padova, Italy
Department of Neuroscience, University of Padova, Padova, Italy
https://orcid.org/0000-0001-8295-3304

Abstract

Purpose: This study evaluates the potential of within-individual Metabolic Connectivity (wi-MC), from dynamic [^{18}F]FDG PET data, based on the Euclidean Similarity method. This approach leverages the biological information of the tracer's full temporal dynamics, enabling the direct extraction of individual metabolic connectomes. Specifically, the proposed framework, applied to glioma pathology, seeks to assess sensitivity to metabolic dysfunctions in the whole brain, while simultaneously providing further insights into the pathophysiological mechanisms regulating glioma progression.

Methods: We designed an index (Distance from Healthy Group, *DfHG*) based on the alteration of wi-MC in each patient (n=44) compared to a healthy reference (from 57 healthy controls), to individually quantify metabolic connectivity abnormalities, resulting in an Impairment Map highlighting significantly compromised areas. We then assessed whether our measure of metabolic network alteration is associated with well-established markers of disease severity (tumor grade and volume, with and without edema). Subsequently, we investigated disruptions in wi-MC homotopic connectivity, assessing both affected and seemingly healthy tissue to deepen the pathology's impact on neural communication. Finally, we compared network impairments with local metabolic alterations determined from SUVR, a validated diagnostic tool in clinical practice.
Results: Our framework revealed how gliomas cause extensive alterations in the topography of brain networks, even in structurally unaffected regions outside the lesion area, with a significant reduction in connectivity between contralateral homologous regions. High-grade gliomas have a stronger impact on brain networks, and edema plays a mediating role in global metabolic alterations. As compared to the conventional SUVR-based analysis, our approach offers a more holistic view of the disease burden in individual patients, providing interesting additional insights into glioma-related alterations.
Conclusion: Considering our results, individual PET connectivity estimates could hold significant clinical value, potentially allowing the identification of new prognostic factors and personalized treatment in gliomas or other focal pathologies.

Running title: Metabolic Connectivity in gliomas

Keywords: Individual-level Metabolic Connectivity; Brain network alterations; Glioma; [^{18}F]FDG dynamic PET; Cancer Neuroscience; SUVR

Introduction

In recent years, the brain has been studied as a complex network comprised of interconnected regions that operate on a large scale, a central concept in the field of neuroscience known as “connectomics”. However, imaging studies on brain connectivity mainly rely on assessing the synchronization of hemodynamic signals obtained through blood oxygen level dependent (BOLD) functional magnetic resonance imaging (fMRI), referred to as Functional Connectivity (FC), and evaluating the number and strength of white matter connections

between brain regions using diffusion magnetic resonance imaging (dMRI) techniques, termed as Structural Connectivity (SC). However, given that chemical synapses are the primary means of signal transduction in the human brain, a pivotal advancement for connectomics involves delving into the molecular aspects of neural communication [1]. At the macroscale level, the exploration of these phenomena is facilitated by molecular imaging. In particular, positron emission tomography (PET) utilizing [^{18}F]fluorodeoxyglucose ([^{18}F]FDG) as a radiotracer offers a unique opportunity to characterize the metabolic foundations of brain connectivity, denoted as "Metabolic Connectivity" (MC), which describes the relationships between the metabolic measurements of different brain regions.

PET connectivity studies typically use static PET data, with pairwise correlations of semiquantitative [^{18}F]FDG uptake measures (e.g., standardized uptake value ratio, SUVR) being computed across individuals, leading to group-level MC matrices [2]. However, this approach encounters a significant constraint, relying on the definition of an homogeneous group of individuals and the normalization of interindividual differences, which significantly restricts the applicability of the method [3]. Moreover, an individual estimate is by definition necessary if one aims to use MC as a disease biomarker [4].

Several approaches have recently been developed with the aim of estimating individual-level MC measures from these group-level matrices, such as the perturbation approach by Sun et al. [5], the Kullback-Leibler divergence similarity estimation by Wang et al. [6], and the method based on a weighting matrix by Huang et al. [7], which mostly work by assessing how much the PET regional data of one individual contribute to the group-level MC matrix, and how the matrix changes when removing a given subject. In addition, such methods rely on static PET images, and thus on a single cumulative measurement of cerebral glucose uptake, not accounting for the temporal dynamics of the network within an individual. When aiming to integrate data from multiple imaging modalities (e.g., fMRI and PET) to provide a more comprehensive understanding of brain connectivity, it is necessary to introduce a method for computing MC that is conceptually comparable to FC, which correlates signal fluctuations between spatially distinct brain regions, taking into account brain dynamics. For this reason, in our previous study we addressed the challenge of selecting an effective approach to derive within-individual MC (wi-MC) starting from dynamic PET data [8], expanding on the previous correlation-based method proposed by Jamadar and colleagues [4]. While the latter was designed for constant-infusion functional PET data, our focus was to propose a method suitable for any protocol, including bolus injection. We developed the Euclidean Similarity (ES) method, based on pairwise Euclidean distance between time-activity curves (TACs), given that

a distance-based approach has long been proven effective in identifying biologically significant clusters in dynamic PET data (i.e. it can reliably differentiate voxels belonging to "functionally" distinct regions of gray matter and white matter according to their different kinetic behaviors) [9]. Importantly, our Euclidean distance-based approach determines similarity based on the amplitude and shape of time-activity curves, which are known to be biologically informative and are therefore used in kinetic modeling, rather than their fluctuations, which are thought to be more related to physical and statistical noise (measurement error) than to biologically informative variability [10]. However, this method has only been applied to a dataset of healthy controls (HCs), and its sensitivity to pathological alterations in metabolic connections within individual brains has not yet been proven.

The present work evaluates the effectiveness of our wi-MC estimation method on a dataset of patients diagnosed with glioma, a primary brain tumor originating from glial cells. On one hand, given the focal nature of glioma pathology, we believe this is an optimal context for testing the efficacy of the method in detecting individual network alterations. On the other hand, this choice is also motivated by the growing clinical interest in the field known as "cancer neuroscience", which aims to understand the complex network of high-level relationships between gliomas and their host (i.e., the brain) [11]. Our goal was to assess whether the wi-MC approach is sensitive to both focal and distant metabolic connection impairments and whether it can provide further insights into the pathophysiological mechanisms regulating glioma progression. These evaluations would offer additional information on disease aggressiveness, enabling individual risk stratification and facilitating personalized treatment strategies.

(1) First, we developed a novel region-wise index (referred to as Distance from Healthy Group, *DfHG*) capable of accurately quantifying the extent of wi-MC alterations in glioma patients and constructed an Impairment Map of significantly altered regions for each individual. (2) Then, we evaluated whether wi-MC impairments are associated with well-established disease severity markers, including tumor grade and volume. (3) Additionally, we investigated if glioma pathology leads to disruption in wi-MC homotopic connectivity. Although the present study represents the first attempt to investigate gliomas within the MC framework, such lesions have already been extensively explored in fMRI FC studies. Strong functional connections between mirror areas in the two hemispheres are considered a key feature of normal brain function, but in glioma patients the pathways that facilitate these communications may be disrupted [12]. (4) Finally, since regions of hypo- or hyper-metabolism, based on SUVR, represent a valuable diagnostic tool for gliomas in clinical practice, our aim was to demonstrate

the added value of wi-MC in characterizing disease-related impairments (i.e., metabolic network alterations), proving its complementarity with information derived from SUVR (i.e., local metabolic alterations) and laying the foundations for potential clinical application of wi-MC.

Materials and methods

Participants

Pre-surgical data of 44 patients (mean age 60.8±14.9 years, 25 males) with *de novo* brain tumors were collected at the University Hospital of Padova between June 2016 and April 2021. Diagnosis was made according to the criteria of the WHO classification system, 2016 version [13]. The dataset includes 6 low-grade gliomas (LGG), 35 high-grade (HGG) and 3 for whom the grading information was not available (biopsy not performed); as to IDH1 mutation status, 28 are wild-type, 5 mutated and 11 undefined. The patients' demographic and clinical information are summarized in **Table 1**. All participants regularly received anticonvulsants for seizure control, and corticosteroids. The protocol has been approved by the local Ethics Committee of the University Hospital of Padova and conducted in accordance with the 1964 Declaration of Helsinki and its subsequent amendments. Written informed consent was obtained from all participants.

The HC group was composed of 57 adults (mean age 55.8±15.2 years, 25 males) as part of the Adult Metabolism & Brain Resilience (AMBR) study [14].

Table 1 Patients' demographics and clinical data

Age (years)	60.8 ± 14.9
Gender	
Female	19
Male	25
Tumor Histology	
Astrocytoma	2
Diffuse astrocytoma	1
Glioblastoma	32
Gliosarcoma	1
Glioneural neoplasm	2
Oligodendroglioma	1
Other	5
Tumor grade	
II	6
III	3
IV	32
n.a.	3

IDH1 mutation status	
Wild-type	28
Mutated	5
n.a.	11
Tumor site	
Left	23
Right	18
Bilateral	3

IDH, isocitrate dehydrogenase gene; n.a., not available

Data acquisition

[^{18}F]FDG PET and structural MRI images were acquired for both patients and controls.

Glioma patients underwent simultaneous PET/MR acquisitions on a Siemens 3T Biograph mMR scanner (Siemens, Erlangen, Germany). Dynamic PET data (60-minute acquisition), performed following an intravenous bolus manual-injection of 203±40 MBq, were reconstructed as 256x256x127 matrices with a 2.8x2.8x2.0 mm^3 voxel size, in 39 frames with increasing duration (10x6 s, 8x15 s, 9x60 s, 12x240 s).

For HCs, structural MRI scans were performed on a Siemens Magnetom Prisma^{fit} scanner, while [^{18}F]FDG scans were acquired on a Siemens 962 ECAT EXACT HR+ PET (Siemens/CTI) scanner. Dynamic PET data (60-minute acquisition), performed following an intravenous bolus manual-injection of 187.7±12.1 MBq, were reconstructed as 128x128x63 matrices with a 2.0x2.0x2.4 mm^3 voxel size in 52 frames (24x5 s, 9x20 s, 10x60 s, 9x300 s). All PET images were acquired in the eyes-closed waking state. For a comprehensive description of the acquisition protocols see **Supplementary Methods**.

MRI preprocessing

T1w structural images of both patients and HC group underwent similar pre-processing procedures, outlined in detail in the **Supplementary Methods**.

The present study employed two distinct parcellation schemes: the Hammers anatomical atlas [15], and the Yan homotopic functional atlas, 100 regions of interest (ROIs) and 7 Networks [16]. Each atlas was registered to individual T1w image using the Advanced Normalization Tools (ANTs, v2.4.3) [17].

Regarding the Hammers atlas, a total of 74 regions were selected for analysis, excluding white matter (WM) and cerebrospinal fluid (CSF) ROIs (list provided in the **Supplementary Methods**).

As to the Yan atlas, the initial set of 100 ROIs was supplemented with 12 additional subcortical regions from the Hammers atlas, including bilateral Caudate, Nucleus accumbens, Putamen, Pallidum, Thalamus, and Cerebellum regions. The atlas-based networks are Default Mode, Cognitive Control, Limbic, Ventral Attention, Dorsal Attention, SomatoMotor, Visual, plus Subcortical and Cerebellum. The Yan atlas results are presented in the main manuscript, while the Hammers results are reported in the **Supplementary Material**.

For glioma patients, we exploited the two lesion segmentations already defined in our previous work [18]: specifically, the tumor (TM) mask includes tumor core (contrast agent enhancing and non-enhancing regions) and necrosis, while the lesion mask (TM+E) also includes the area of edema (E). In the patient group, all the normalizations to the standard space were performed with ANTs [17] excluding the TM+E area [19].

PET analysis

The dynamic PET data of both patients and HCs underwent motion correction using FSL's *mcflirt* algorithm [20], and to minimize partial volume effects (PVEs), the data were processed without applying any additional spatial smoothing, in agreement with many recent studies [21]. For each participant, a static PET image was generated by summing the motion-corrected late PET frames (40-60 min) and the static PET was registered to the T1w image using ANTs [17]. Finally, the TM and TM+E masks, Hammers and Yan parcellations, and the individual grey matter (GM) and white matter (WM) tissue segmentations, obtained using Statistical Parametric Mapping tool (SPM12, v7219 https://www.fil.ion.ucl.ac.uk/spm/), were mapped from T1w to PET space, applying the previously estimated transformations. Subsequently, the static PET image of both patient and HC was normalized by dividing each voxel's value by the average [^{18}F]FDG uptake in the Cerebellum WM (as further described in the **Supplementary Methods**), resulting in SUVR map [22]. In the case of healthy individuals, the reference region comprises the bilateral Cerebellum WM. For glioma patients, the reference region encompasses the Cerebellum WM ipsilateral to the lesion (except for those with bilateral tumors, where the bilateral Cerebellum WM is used). This choice was motivated by the fact that the incidence of glioma is very low in the cerebellum (4.5% of all gliomas) and crossed cerebellar diaschisis is not infrequent in glioma patients [23].

For each patient/control, the SUVR maps were parceled using both Hammers and Yan atlases, i.e. the mean SUVR for each ROI was calculated by averaging the voxels values within the parcel filtered using the GM mask. Note that in the patient cohort, the tumor voxels (TM mask,

mapped to the PET space) were excluded from the regional SUVR computation, as typically done in several studies on gliomas to ensure that possible alterations were not simply due to tumor-associated tissue loss and dysfunction [24].

Tissue TACs were extracted from pre-processed dynamic [^{18}F]FDG PET images – for each ROI belonging to the two parcellation schemes – by averaging the voxel activities within the GM mask (properly described in the **Supplementary Methods**). As for the SUVR, in the calculation of the patients' ROI TACs, tumor voxels (TM mask, mapped to the PET space) were excluded, as done for regional SUVR values. Regional TACs were then interpolated on a uniform virtual grid (one-second step) and wi-MC matrices were calculated for both HCs and patients, using a the ES-based method, detailed in Volpi et al. [8] and summary reported in the **Supplementary Methods.**

Calculation of the *DfHG* index in Glioma patients

To evaluate the capability of wi-MC matrices to discriminate pathological changes in brain metabolic connections caused by glioma, we introduced a novel index designed to quantify regional impairment for each patient. The analysis workflow is reported in **Fig. 1**. For this purpose, a healthy wi-MC reference was first defined by averaging the wi-MC matrices obtained from the 57 HCs. As previously shown, the ES approach leads to a robust estimate of group-average wi-MC in HCs: the between-individual variability is low, so the average matrix can be considered as well-representative of the HC group [8].

For each participant (patient or control), we defined a region-wise index (referred to as **Distance from Healthy Group, *DfHG***), which involves calculating the Pearson's correlation coefficient (r_i, range [-1, 1]) between the wi-MC profile of the i-th ROI in the individual (x_i) and the corresponding ROI profile in the HC reference template (y_i). Only regions with significant correlations (after Bonferroni correction) were selected for further analysis. Finally, the index for each individual's i-th ROI was defined as one minus the correlation value ($DfHG_i$, range [0, 2]). Since no alterations are expected in wi-MC among HCs, the values of the *DfHG* index from all ROIs across individuals were collectively utilized to establish a healthy reference distribution. Subsequently, for each glioma patient, a region-by-region analysis was conducted by comparing the *DfHG* calculated for each region with the healthy reference distribution: a ROI was deemed impaired if its *DfHG* value exceeded the 97.5th percentile of the healthy distribution. This highly conservative threshold was chosen to ensure selectivity in the identification of significantly compromised regions, minimizing the risk of false positives.

A sensitivity analysis was also performed to verify the impact of the threshold in the selection of affected areas (see **Supplementary Methods**).

Finally, an *Impairment Map* was generated for each patient from the abnormal ROIs according to the above-mentioned procedure.

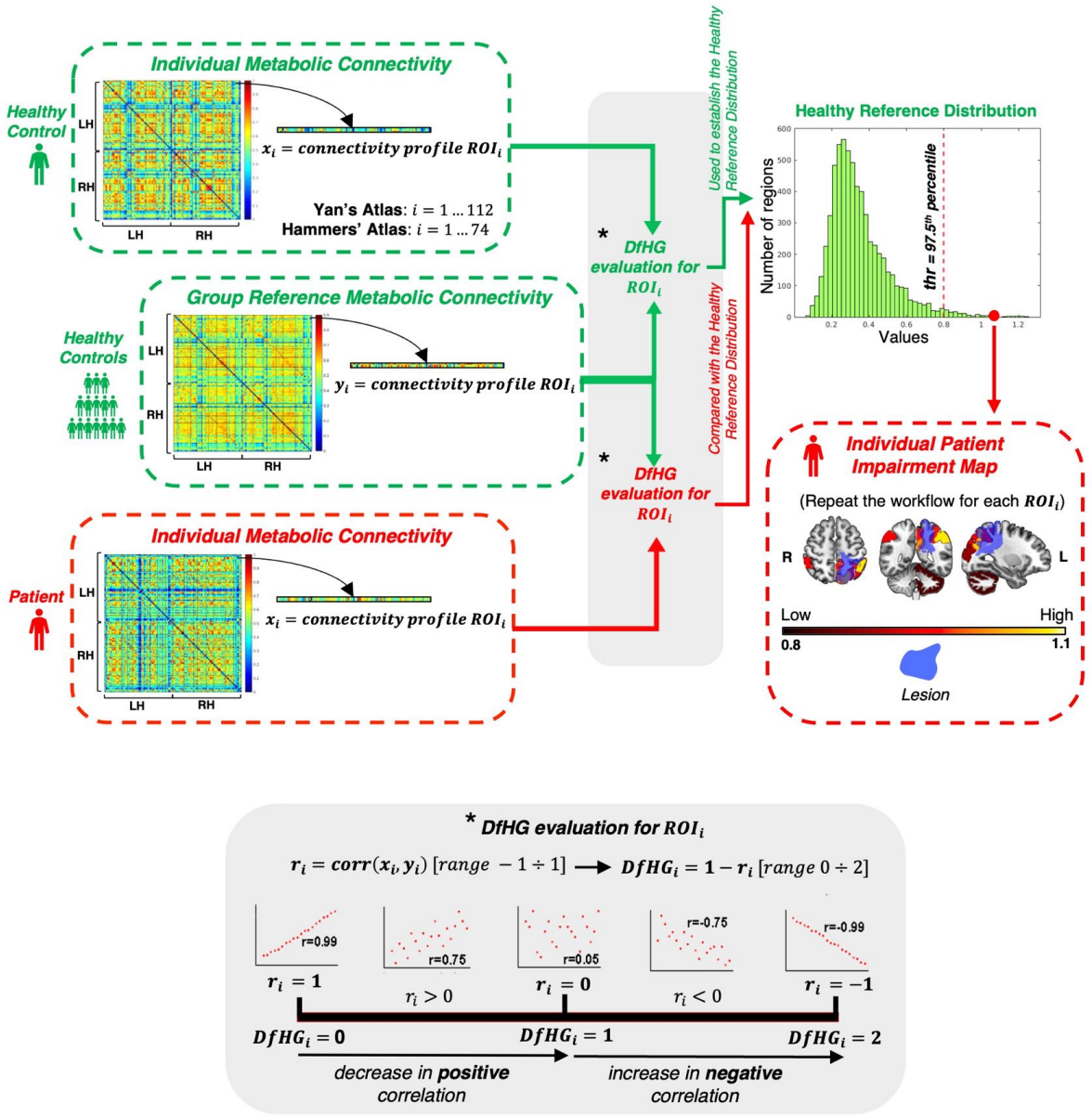

Fig. 1 The wi-MC matrix is calculated for each participant (both healthy controls and patients). The *Group Reference Metabolic Connectivity* is obtained as the average of the wi-MC matrices of the healthy controls only. The *DfHG* index values from all regions and all healthy individuals were collectively used to establish the *Healthy Reference Distribution*. Subsequently, in each glioma patient, the *DfHG* index for each region is computed and compared with the *Healthy Reference Distribution*: if the *DfHG* exceeds the 97.5th percentile threshold of the healthy distribution, the region is marked as impaired and included in the patient's Impairment Map

(i.e., all the regions deemed as impaired in a given patient). The lower panel describes the *DfHG* calculation for the i-th ROI: for each ROI, the Pearson's correlation (r_i) between the wi-MC connectivity pattern of the i-th ROI in the individual participant (x_i), i.e., the i-th row in the wi-MC matrix, and the wi-MC connectivity pattern of the same i-th ROI in the group reference MC matrix (y_i) is calculated; the $DfHG_i$ index is obtained as one minus r_i. The relation between the values of Pearson's correlation (r_i) and the derived index $DfHG_i$ is also described in the lower part.

Association between Overall Impairment and markers of disease severity

We then examined whether the *DfHG* index estimated from the patient's wi-MC correlates with known markers of disease severity in gliomas (lesion volume, grade). The patient's *Overall Impairment* (OI) was derived by averaging the *DfHG* indices across all brain regions, offering a global assessment of the wi-MC alterations induced by glioma. We then investigated the across-individual association between OI and tumor grade, as well as the volume of both the entire lesion (TM+E) and the tumor (TM). Specifically, the Mann-Whitney U-test ($P<0.05$) was employed to compare the OI between patients with high-grade (HGG, n=35) and low-grade glioma (LGG, n=6). The Mann-Whitney U-test was chosen due to the non-normal data distributions revealed by the Lilliefors test. A linear regression analysis was performed to assess the relationship of OI with TM+E and TM volume. Particularly, for the analysis of the association between OI and grade, the 3 patients with unavailable grade information were excluded from the analysis, whereas the volumes of TM+E and TM are available for all 44 patients.

Homotopic Connectivity

To examine the disruption of homotopic connectivity induced by gliomas, we also assessed the presence of reduced wi-MC between homologous areas, akin to previous approaches employed in fMRI FC studies [12]. For each pair of homotopic regions (mirror areas of the two hemispheres, 37 pairs in the Hammers atlas and 56 pairs in the Yan atlas), the expected distribution of connections was calculated from the HC wi-MC links. Subsequently, the homotopic wi-MC values were extracted for each patient, and a region-by-region comparative

analysis was conducted using the ROI-specific HC distribution as a reference. Region pairs were categorized into two types: those involving ROIs of apparently normal tissue and those in which one region overlaps with the lesion (TM+E). Subsequently, global homotopic connectivity, computed as the average of all homologous pair wi-MC values, was compared between LGG (n=6), HGG (n=35) and HCs (n=57) using a one-way ANOVA and Tukey-Kramer's test to address multiple comparisons, chosen due to the normal data distributions revealed by the Lilliefors test. Finally, a linear regression analysis was performed to assess the relationship of the global homotopic connectivity with TM+E and TM volume.

SUVR impairments

To identify regions whose local metabolism is altered, we performed a statistical comparison on SUVR maps at the region level between each patient and the control group. First, the parceled SUVR values of each HC underwent a z-score transformation (z-SUVR) to remove inter-individual differences of tracer uptake in mean and standard deviation (SD), as in Horwitz et al. [25]. For each ROI, we defined the expected distribution of z-SUVR values in HCs, and we set an abnormality threshold, comparable to the one chosen for wi-MC *DfHG* indices. Since z-SUVR values approximately follow a Gaussian distribution, with alterations manifesting as hypo- or hyper-metabolism, we established thresholds for both tails of the distribution, encompassing 97.5% of the values within this range. A z-score transformation was also performed for each patient but considering only regions in the hemisphere contralateral to the tumor for the calculation of the mean and SD values, to avoid the results being affected by large lesions. For the three patients with bilateral gliomas, the predominant hemisphere and tumor-involved regions in the contralateral hemisphere were excluded from the calculation of mean and SD of z-SUVR. We then compared the z-SUVR value of each ROI in each patient with the region-specific healthy reference distribution, marking the region as metabolically impaired if it exceeded the established thresholds. As for wi-MC *DfHG* indices, a sensitivity analysis was performed to verify the impact of the threshold in the selection of metabolically compromised areas (see **Supplementary Methods**).

Results

Participants

The lesion frequency maps (TM+E and TM) of the patient population are shown in **Supplementary Fig. 1**. The lesion distribution is sparse, with tumors predominantly involving the right frontal and temporal lobes, with low spatial overlap (maximum value 21.9% of patients for TM+E and 17.1% of patients for TM).

Impairment Maps

The Impairment Maps generated for 4 representative patients are shown in **Fig. 2**, where the TM+E mask is highlighted in blue, and the *DfHG* values of the significantly altered ROIs (Yan atlas), going from low (dark) to high (light), are reported. The Hammers version is shown in **Supplementary Fig. 5**. From visual inspection, it is evident that in all individuals there are compromised regions which overlap with the lesion areas. However, the impacted ROIs are not confined to the lesioned tissue, with alterations in wi-MC that extend into uninjured brain areas in both the ipsilateral and contralateral hemisphere. For example, patient 7 (Pt #07) has a HGG in the left parietal lobe, which is well detected by its Impairment Map. Patient 12 (Pt #12) has a HGG in the left temporal lobe, while patient 24 (Pt #24) has a HGG in the right fronto-insular area; in both cases the lesions are detected by the wi-MC analysis. In all three patients, there are several compromised areas that spread beyond the tumor itself into structurally unaffected regions (outside the lesion) of the tumor-bearing hemisphere, ipsilateral cerebellum, and the contralateral hemisphere. The involvement of non-lesioned brain tissue is much less pronounced in LGGs, as evident in patient 2 (Pt #2). In this case, the disturbances in wi-MC are confined to the tumor ROIs, with an almost intact pattern in the non-injured tissue. Notably, the patients' *DfHG* values observed in our data have a range between 0.1 and 1.4, which correspond to correlation values ranging from -0.4 ($DfHG_i = 1.4$) to 0.9 ($DfHG_i = 0.1$).

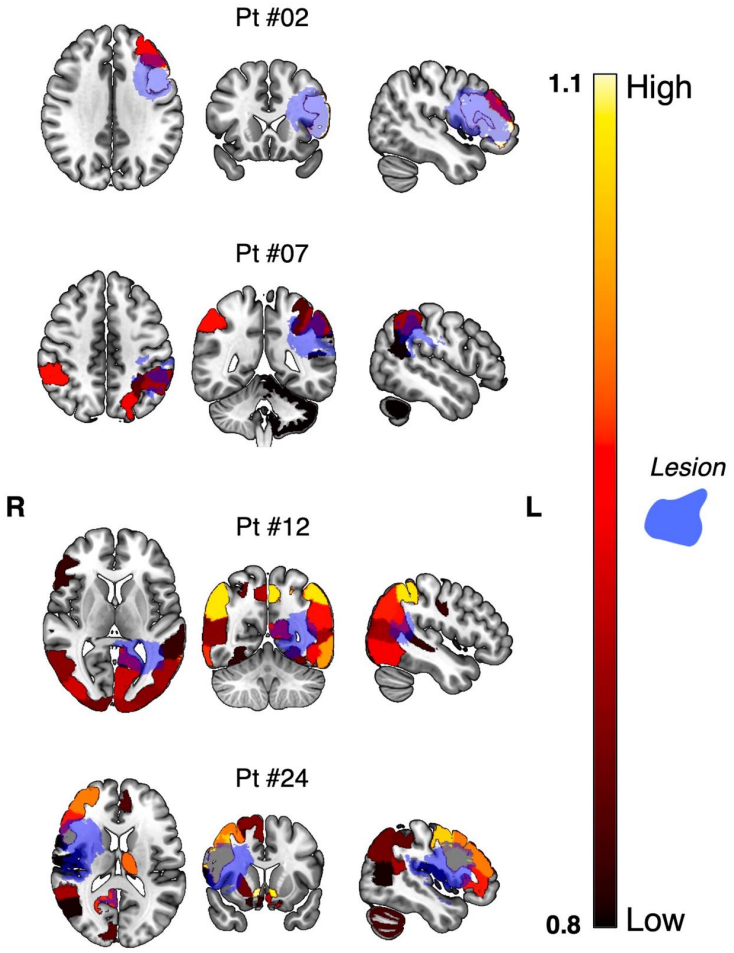

Fig. 2 The lesion mask is shown in blue, the altered ROIs (Yan atlas) are shown according to their *DfHG* value, from low (dark) - small impairment values - to high (light) - increased impairment values. Pt #02 has a low-grade glioma in the left frontal lobe; Pt #07 has a high-grade glioma in the left parietal lobe; Pt #12 has a high-grade glioma in the left temporal lobe and Pt #24 has a high-grade glioma in the right fronto-insular area

Association between Overall Impairment and markers of disease severity

Fig. 3 depicts the relationships of the Overall Impairment (OI) index (Yan atlas) with the entire lesion (TM+E) volume (**Fig. 3a**) and the tumor (TM) volume (**Fig. 3b**). In both cases a significant correlation is observed, with a stronger association when including edema (lesion: R^2=0.53, P<0.001; tumor: R^2=0.35, P<0.001). Patients with low-grade glioma (**Fig. 3,** *black-filled dots*) have the lowest values of OI: this observation is confirmed via the Mann-

Whitney U-test, which revealed HGG patients having a significantly higher OI index than LGG ($P<0.001$).

The Hammers atlas results corroborate these findings: a significant relationship is identified between OI and both lesion ($R^2=0.52$, $P<0.001$) and tumor volume ($R^2=0.34$, $P<0.001$), and a significant difference in OI between HGG and LGG is detected (Mann-Whitney U-test, $P<0.001$).

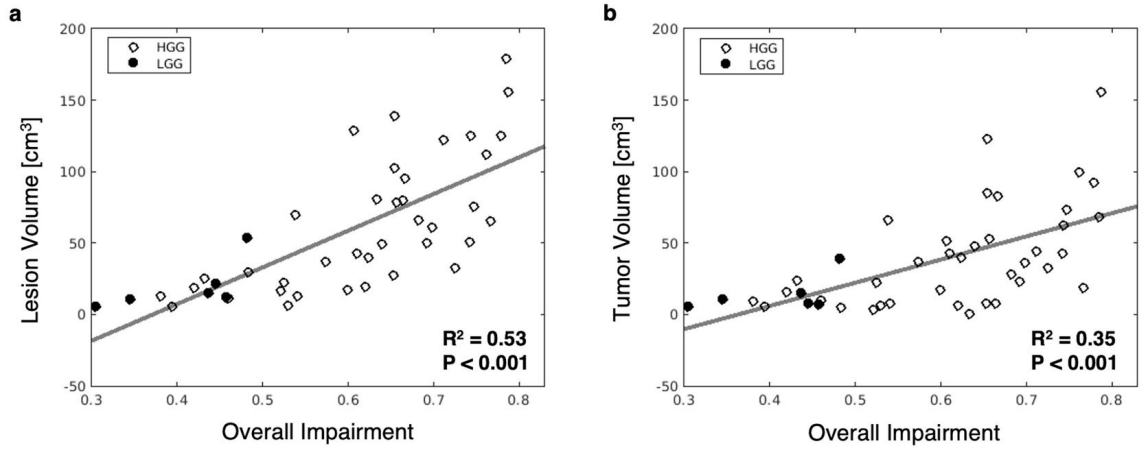

Fig. 3 Scatter plots reporting the association between the Overall Impairment index and (**a**) lesion volume (tumor and edema) and (**b**) tumor volume (without edema), on the Yan functional atlas. HGG patients are shown as empty dots, LGG patients as black-filled dots

Homotopic Connectivity

Fig. 4a shows the homotopic connectivity values of two representative patients (patient 3 has a HGG and patient 20 has a LGG) in two distinct homotopic regions (Yan atlas), along with the distribution of the corresponding homotopic connection values in HCs. Specifically, one pair comprises ROIs of normal-appearing tissue (*right column*), while the other pair includes a region that overlaps with the lesion site (*left column*). A notable observation is the substantial difference in homotopic connectivity between HGG and LGG patients. While in the former, the decrease in connectivity between contralateral homologous regions is not only evident in areas directly impacted by the pathology but also in tumor-free ROIs, in the latter, values remain within the HCs distribution. To gain a comprehensive understanding of the phenomenon, the global homotopic connectivity values for HCs, LGGs and HGGs is also reported in **Fig. 4b**. The one-way ANOVA revealed a significant difference in global homotopic connectivity between the three groups ($P<0.001$). Tukey-Kramer's post hoc test for

multiple comparisons suggested a significant decrease in connectivity within contralateral homologous regions between HCs and HGGs ($P<0.001$), as well as between LGGs and HGGs ($P<0.05$), but no significant difference was observed between HCs and LGGs ($P=0.95$) confirming the observations we derived from panel (**a**). Finally, to further investigate the association between global homotopic connectivity and glioma severity, we assessed the potential effects of tumor volume, both in terms of TM+E and TM. In both cases, no significant relationship was found (TM+E: $R^2=0.05$, $P=0.134$; TM: $R^2=0.04$, $P=0.194$).

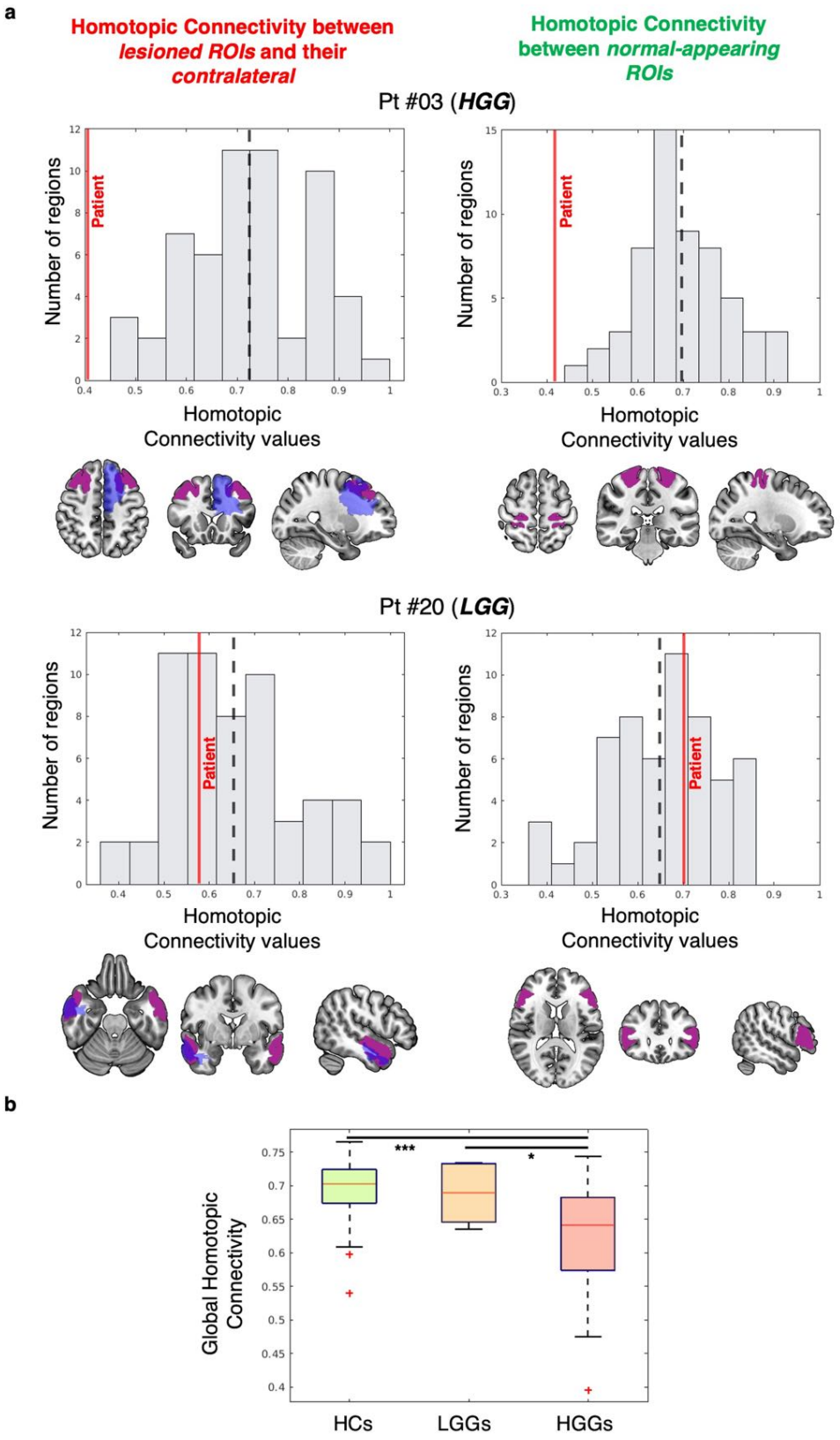

Fig. 4 (**a**) Homotopic connectivity values (red line) of two representative patients (Pt #03 - high-grade - and Pt #20 - low-grade) in two distinct pairs of regions (Yan atlas regions in pink, lesions in blue). Regions with no overlap with the lesion are reported on the right, regions that

overlap with the lesion on the left. For Pt #03, we selected an area within the Default-Mode network on the left, and an area within the SomatoMotor network on the right. Regarding Pt #20, an area within the Default Mode network (temporal) was identified on the left, and an area within again the Default Mode network (prefrontal cortex) on the right. The distribution of the corresponding homotopic connectivity values in HCs is reported in the histograms (dashed black line represents the HCs mean). (**b**) Boxplots with global homotopic connectivity values for HCs (green), LGGs (yellow) and HGGs (red). ***P < 0.001; *P < 0.05

SUVR and wi-MC impairments

Fig. 5a reports the impaired regions (*rows*), grouped according to Yan atlas networks plus Subcortical areas and Cerebellum, for each patient (*columns*). The matrix distinguishes between SUVR-only impairments (*green*), wi-MC-only impairments (*orange*), and regions where both SUVR and wi-MC exhibit alterations (*purple*). Notably, the figure highlights how network alterations (as determined from wi-MC) and local metabolic changes (SUVR) show only partially overlapping areas, with distinct regions affected by each process. Specifically, wi-MC shows a considerable number of impairments in the Default Mode, Cognitive Control, Subcortical, Cerebellum and Visual network areas.

Moreover, patients with tumors in the right hemisphere seem to exhibit more pronounced network alterations compared to those with left-sided lesions: the proportion of wi-MC alterations among left-sided patients is 11%, whereas it rises to 19% among those with right-sided tumors. This disparity is also evident in SUVR alterations, albeit to a lesser degree, with rates of 12% for left-sided gliomas and 15% for right-sided ones.

The role of the cerebellum is also noteworthy: the ipsilateral cerebellum is impaired in 41% and 29% of patients in terms of wi-MC and SUVR, respectively, while the contralateral cerebellum exhibits impairment in wi-MC for 19% and in SUVR for 14% of patients.

Fig. 5b reports the network-wise percentage of altered regions, in terms of only wi-MC, only SUVR, and both SUVR and wi-MC, relative to the total number of alterations in the network. Many overlapping impairments emerge in the Dorsal Attention, Default Mode, Cognitive Control network, and Cerebellum. The remaining networks instead show complementarity between the two types of metabolic alterations.

Fig. 6 shows Impairment maps in terms of SUVR (*green*), wi-MC (*orange*), and both SUVR and wi-MC (*purple*) for four representative individuals. From the SUVR alteration maps, it is evident that local impairments are primarily confined to the lesion area and adjacent regions.

Impairments based on wi-MC, on the other hand, highlight not only proximal but also distant areas from the lesion, both in the ipsilateral and contralateral hemispheres.

The Hammers results are shown in **Supplementary Fig. 6**. The complementarity of the alterations highlighted by the network-based and local approach is again evident, with a greater overlap in Frontal and Parietal areas.

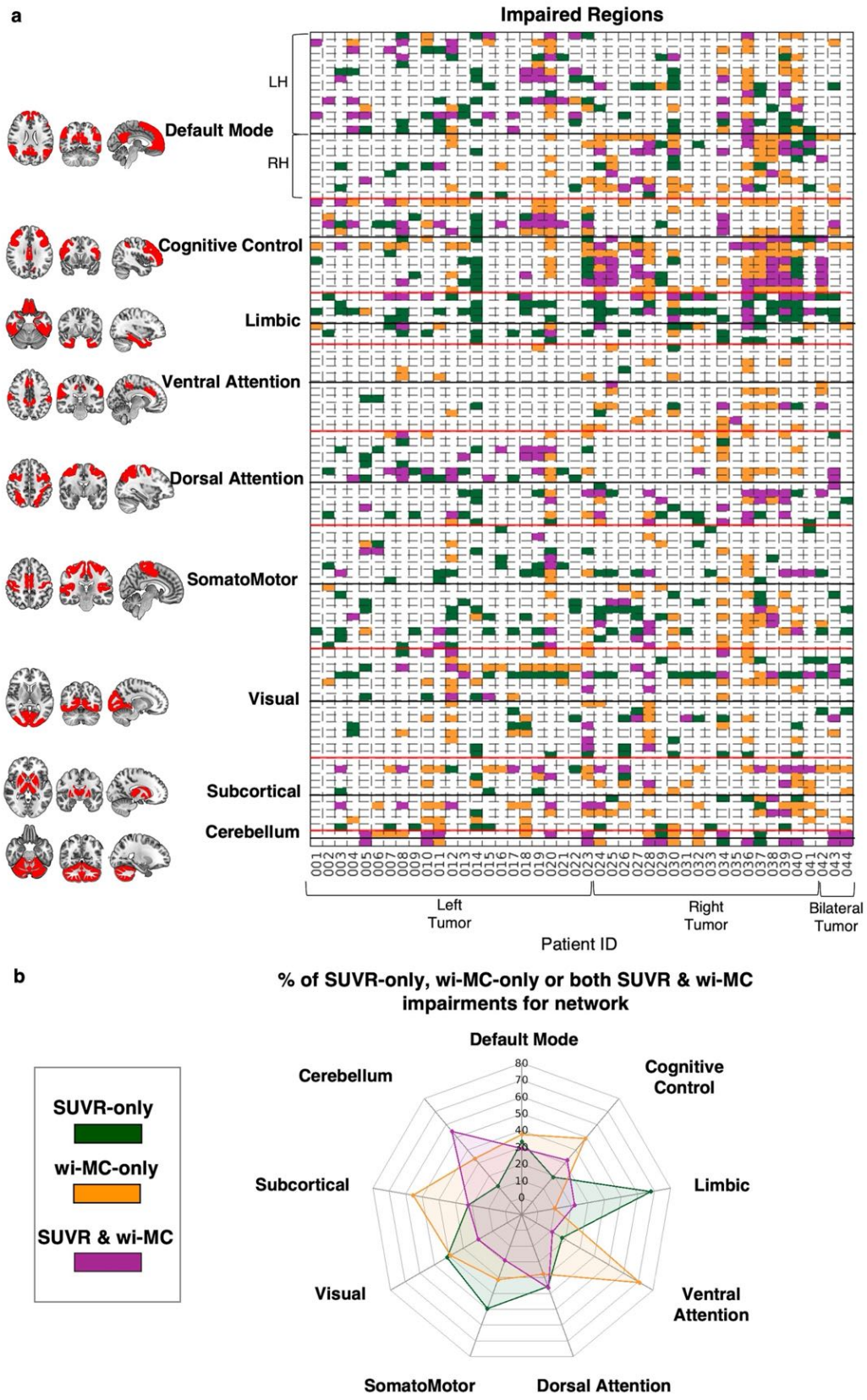

Fig. 5 (**a**) Altered regions according to SUVR-only (green), wi-MC-only (orange), both SUVR and wi-MC (purple) are reported (rows) for each individual patient (columns). Participants are sorted into patients with lesions in the left hemisphere (Left Tumor), patients with lesions in

the right hemisphere (Right Tumor), and patients with bilateral lesions (Bilateral Tumor). The regions are organized by network (visualized on the left). (**b**) Spider plot representing the percentage of altered regions by type (SUVR-only, wi-MC-only, both SUVR and wi-MC) over the total number of altered regions per network

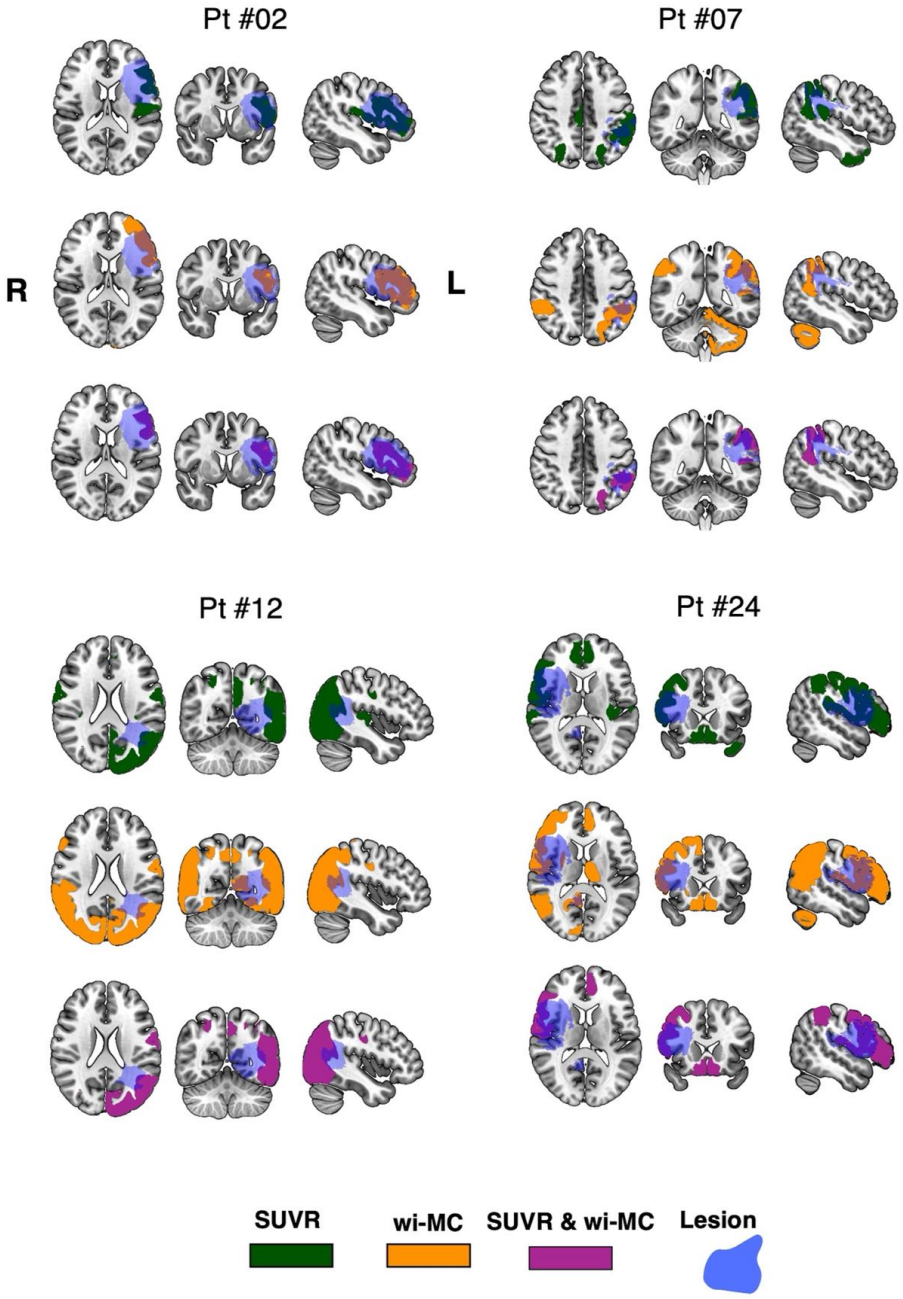

Fig. 6 Impairment map of SUVR (local impairment, green), wi-MC (network impairment, orange) and the overlap of SUVR and wi-MC (both local and network impairment, purple)

Discussion

This study aimed to evaluate the potential of within-individual metabolic connectivity (wi-MC) based on the Euclidean Similarity (ES) method, which, for the first time, leverages the biological information of the tracer's full temporal dynamics, enabling the direct extraction of individual metabolic connectomes [8]. Specifically, the proposed framework applied to glioma pathology (lesions highly localized in patients but heterogeneous across individuals, unlike neurodegenerative disorders, for instance), seeks to assess sensitivity to metabolic dysfunctions at whole-brain level and simultaneously provide further insights into the pathophysiological mechanisms regulating glioma progression.

We first derived a novel imaging marker for each brain region, i.e., the *DfHG* index, from the individual metabolic connectome of every patient. The proposed marker is not based on local metabolism, but rather on the interaction of each region with all other brain areas (the region's "connectivity profile"), and thus captures the impact of the tumor on the brain's entire metabolic architecture. By focusing on regions with a *DfHG* index higher than the normality threshold, we have built an Impairment Map for each patient. Upon visual inspection, it is clear that the areas affected by the presence of the lesion show the expected wi-MC alterations, which is the first important finding, because it confirms that the proposed method is sensitive to connectivity changes and that the obtained brain's MC structure is disrupted as expected in the areas directly impacted by the lesion.

The second key finding is that metabolic network abnormalities do not just fall in the region of tumor-related structural damage, or even in the much larger region of edema. The presence of dysfunction in brain areas remote from the primary injury is referred to as diaschisis [26]. This is evident from the impairment maps shown in **Fig. 2**, in which alterations also emerge in apparently healthy tissue (i.e. beyond the region outlined in the lesion map), both ipsilaterally and contralaterally. This can be linked to three mechanisms. Firstly, substantial interactions between the neural system and malignant cells have been proven to exist, occurring not only near the tumor site but also at a distance, with glioneuronal synapses that enable gliomas to integrate into functionally active brain circuits [27]. Secondly, at least in some specific patients, the compromise of apparently healthy tissue could be attributed to the direct involvement of the anterior commissure, which, together with the corpus callosum, serves as an important conduit for interhemispheric information transfer. This results in a direct disruption of essential connections necessary for promoting optimal brain functionality. Indeed, this is the case of patient 12 (**Fig. 2**), wherein there is clear involvement of the anterior commissure in the tumor,

and in fact, the metabolic connectome alterations are widely distributed across areas in the contralateral hemisphere. However, it should be noted that the altered areas do not always follow the well-known anatomical connections with the lesion site. We believe this may be due to the only partial matching between metabolic and structural connectomes [8] as well as mechanisms of metabolic network reorganization and metabolic compensation, a concept previously highlighted in functional connectivity studies [28]. Finally, the lesion may decrease the functionality of a specific area, thereby hindering the transfer of information and interactions with other regions, leading to anomalies even in anatomically distant but metabolically related areas. This latter mechanism could explain alterations especially in homotopic connectivity (i.e., robust and strong associations between mirror areas of the two hemispheres), which is a common feature of healthy brains [12]. However, our findings (**Fig. 4**) suggest that tumor grade potentially plays a significant role in distorting homotopic connectivity in glioma patients. Intriguingly, low-grade gliomas (LGGs) disrupt communications between these regions to a lesser extent than high-grade gliomas (HGGs), and this observation applies to pairs of regions affected by the lesion and to pairs of apparently healthy tissue areas, without identifying any volume-dependent association, in agreement with the fMRI FC findings of Daniel and colleagues [12]. This is the case of patient 2 (**Fig. 2**), LGG, who presents few alterations, which are limited to the area of the lesion. This finding aligns with previous studies which emphasized that 1) regions within the tumor boundaries in LGGs tend to preserve their functionality, potentially leading to less extensive alterations and 2) that HGGs exhibit more significant tumor cell invasion with respect to LGGs [24]. The latter could explain the greater MC impairment observed in HGGs in multiple distant sites and resting-state networks. Based on this, we tested whether the patient's Overall Impairment (OI), defined as the average *DfHG* index across regions, was associated with known markers of disease severity, such as lesion grade and volume. This index enables a comprehensive evaluation of the pathology's impact on the patient's metabolic brain architecture. It considers not only the significantly affected areas, which contribute to the Impairment Map, but also the degree of alteration in the remaining regions. Thus, a high OI value (close to 1) suggests extensive impairment, with many regions showing high levels of alteration, while a low OI value (close to 0) suggests limited alteration confined to a few regions, with most ROIs retaining a pattern similar to that of a healthy brain. In terms of lesion grade, this analysis confirmed that not only from the perspective of homotopic connectivity, but also regarding OI, LGGs exhibit greater integrity in the cerebral metabolic connectome compared to HGGs (**Fig. 3**). We also found a strong association of OI with both tumor volume (TM) and lesion volume (TM+E).

Importantly, this relationship becomes significantly stronger when taking edema into account, suggesting that the edema region may play a crucial role in modulating brain function in glioma patients, contributing to the observed changes in the OI. The result is supported by studies highlighting how glioma-related edema promotes cell invasion and markedly influences disease prognosis, contributing significantly to morbidity and mortality from glioma [29]. To our knowledge, this study is the first to unveil the role of edema in contributing to the alteration of the brain connectome in glioma pathology.

Finally, we aimed to demonstrate the added value of the proposed approach, which is based on analyzing the individual patient's metabolic connectome, with respect to conventional clinical methods based on the patient's SUVR map. These two approaches give different perspectives: the former highlights large-scale network alterations, while the latter focuses on local changes. As visible in **Fig. 5**, the two methodologies only have a partial overlap, suggesting they could be complementary for reaching a comprehensive understanding of the pathology. While the relatively high occurrence of tumors in frontal regions helps explain the greater overlap of MC and SUVR alterations in Default Mode and Cognitive Control network areas, the substantial involvement of the Cerebellum is particularly surprising. This would suggest that its gray matter metabolism, and its connectivity pattern even more (i.e., the way it interacts with the remaining cortical and subcortical regions), are severely disrupted by glioma pathology. One potential reason for the elevated incidence of cerebellar alterations may stem from the well-known presence of connections between cortical areas—namely, the parietal, prefrontal, and temporal cortices—and the cerebellum, as evidenced by structural [30] and magnetic resonance imaging studies [31]. Therefore, the presence of cortical lesions could certainly have consequences on normal metabolic mechanisms (both local and connectivity-related) involving the cerebellum. This is a new finding for [^{18}F]FDG PET imaging, whereas Nenning and colleagues have already observed a highly symmetrical functional abnormality in glioma pathology, affecting not only cerebral but also cerebellar regions, irrespective of being ipsi- or contralateral to the tumor [32]. The frequent MC impairment of visual network components is also noteworthy, given that the occipital lobe is the least structurally involved by gliomas and farthest from the more commonly affected frontal and temporal areas. Interestingly, this network had previously emerged as highly impaired in a fMRI FC study on the same glioma dataset, which aligns with our current findings [18]. Moreover, patients with right-sided gliomas exhibit a greater disruption of the metabolic connectome. This is well explained by the fact that malignant brain tumors involving the right hemisphere are associated with more subtle symptoms that are difficult to recognize, which translates into a delayed diagnosis and,

consequently, larger tumor volumes and greater impact on brain network architecture at the time of initial diagnosis [33]. Additionally, in the **Supplementary Material**, we investigated the relationship between SUVR alterations and clinical variables such as tumor grade and volume. While LGG patients demonstrated significantly lower SUVR alterations compared to HGGs (Mann-Whitney U-test, $P<0.001$), no significant relationship emerged with lesion volume, contrary to wi-MC. Overall, as evidenced by these examples, our wi-MC approach seems to provide interesting additional insights into glioma-related alterations that are not visible to conventional SUVR analysis.

With respect to study limitations, the number of LGGs (n=6) and HGGs (n=35) in the available glioma dataset is unbalanced, which may affect the reproducibility of the results. Therefore, more in-depth analyses with comparable sample sizes should be conducted in the future to confirm these findings. Additionally, data from patients and controls were acquired with two different scanners, and this may have an impact on the results; we have detailed in the **Supplementary Material** how these differences do not impact the contrast-to-noise ratio of the data. Also, we have not directly compared our wi-MC characterization of glioma patients against the methods that have been previously proposed to "individualize" group-level MC matrices [5–7]. However, all these approaches are still exploratory and require further validation [1], so we chose to compare our wi-MC method only with well-established SUVR-based analysis. Additionally, we aimed to assess the biological information contained in dynamic PET data by testing an approach more akin to the fMRI FC, which relies on the temporal relationship between regional signals measured in the single individual.

Future directions may involve comparing alterations in both metabolic and functional connectivity networks to better understand the effects of glioma pathology. Additionally, analyzing the relationship between Overall Survival and our measure of metabolic connectome alteration index could be of interest, albeit not feasible here due to the limited sample size. Finally, it might be of interest to move analysis to the voxel-level for future individual-level metabolic connectivity research. However, several issues must first be considered and addressed. Firstly, it should be noted that voxel-level analyses would preclude the generation of voxel-to-voxel connectivity matrices akin to those presented in this study (i.e., using the Euclidean similarity method), due to the excessive computational burden this would entail. An entirely different approach would likely be required, e.g., independent component analysis (ICA) [2]. Moreover, the low signal-to-noise ratio of PET data at the voxel level when using data from low-sensitivity clinical scanners must be considered. Therefore, future efforts would

first involve evaluating appropriate noise reduction methodologies to analyze PET data at the voxel-level without introducing significant bias in the MC estimates.
Hence, given these encouraging results, individual PET connectivity estimates could provide important information on in vivo pathological brain features, potentially paving the way for improved treatment and prognosis of gliomas and other focal pathologies.

Statements and Declarations

Funding

The author(s) disclosed receipt of the following financial support for the research, authorship, and/or publication of this article: Funding for this research was provided by the McDonnell Center for Systems Neuroscience and the NIH/ NIA R01AG053503 (AGV) and R01AG057536 (AGV, MSG). Some of the MRI sequences used were obtained from the Massachusetts General Hospital.

Competing interests

The authors declare no potential conflicts of interest with respect to the research, authorship, and/or publication of this article.

Ethics approval

All assessments and imaging procedures were approved by Human Research Protection Office and Radioactive Drug Research Committee at Washington University in St. Louis (healthy controls). Concerning glioma patients, the protocol has been approved by the local Ethics Committee of the University Hospital of Padova. All procedures performed in studies were conducted in accordance with the 1964 Declaration of Helsinki and its subsequent amendments.

Consent to participate

Informed written consent was obtained from all individual participants included in the study.

Consent to publish

Participants signed informed consent regarding publishing their data.

Data availability

The data that support the findings of this study are available from the corresponding author, upon reasonable request.

Author Contributions

Andrei G. Vlassenko and Diego Cecchin collected the data. Giulia Vallini and Alessandra Bertoldo designed the research. Giulia Vallini, Erica Silvestri and Tommaso Volpi analyzed the data. Giulia Vallini, Erica Silvestri, Tommaso Volpi, John J. Lee, Andrei G. Vlassenko, Manu S. Goyal, Diego Cecchin, Maurizio Corbetta and Alessandra Bertoldo interpreted the results. Giulia Vallini wrote the manuscript. All authors revised the manuscript.

References

[1] Sala A, Lizarraga A, Caminiti SP, et al. Brain connectomics: time for a molecular imaging perspective? Trends Cogn Sci. 2023;27(4):353–66. https://doi.org/10.1016/j.tics.2022.11.015

[2] Yakushev I, Drzezga A, Habeck C. Metabolic connectivity: Methods and applications. Curr Opin Neurol. 2017;30(6):677–85. https://doi.org/10.1097/WCO.0000000000000494

[3] Veronese M, Moro L, Arcolin M, et al. Covariance statistics and network analysis of brain PET imaging studies. Sci Rep. 2019 Dec 1;9(1). https://doi.org/10.1038/s41598-019-39005-8

[4] Jamadar SD, Ward PGD, Liang EX, et al. Metabolic and Hemodynamic Resting-State Connectivity of the Human Brain: A High-Temporal Resolution Simultaneous BOLD-fMRI and FDG-fPET Multimodality Study. Cereb Cortex. 2021 May 10;31(6):2855–67. https://doi.org/10.1093/cercor/bhaa393

[5] Sun T, Wang Z, Wu Y, et al. Identifying the individual metabolic abnormities from a systemic perspective using whole-body PET imaging. Eur J Nucl Med Mol Imaging. 2022;49(8):2994–3004. https://doi.org/10.1007/s00259-022-05832-7

[6] Wang M, Jiang J, Yan Z, et al. Individual brain metabolic connectome indicator based on Kullback-Leibler Divergence Similarity Estimation predicts progression from mild

cognitive impairment to Alzheimer's dementia. Eur J Nucl Med Mol Imaging. 2020;47(12):2753–64. https://doi.org/10.1007/s00259-020-04814-x

[7] Huang SY, Hsu JL, Lin KJ, et al. A Novel Individual Metabolic Brain Network for 18F-FDG PET Imaging. Front Neurosci. 2020;14(May):1–11. https://doi.org/10.3389/fnins.2020.00344

[8] Volpi T, Vallini G, Silvestri E, et al. A new framework for metabolic connectivity mapping using bolus [18F]FDG PET and kinetic modelling. J Cereb Blood Flow Metab. 2022;1–21. https://doi.org/10.1177/0271678X231184365

[9] Liptrot M, Adams KH, Martiny L, et al. Cluster analysis in kinetic modelling of the brain: A noninvasive alternative to arterial sampling. Neuroimage. 2004;21(2):483–93. https://doi.org/10.1016/j.neuroimage.2003.09.058

[10] Bertoldo A, Rizzo G, Veronese M. Deriving physiological information from PET images: From SUV to compartmental modelling [Internet]. Vol. 2, Clinical and Translational Imaging. Springer-Verlag Italia s.r.l.; 2014. p. 239–51. https://doi.org/10.1007/s40336-014-0067-x

[11] Mancusi R, Monje M. The neuroscience of cancer. Nature. 2023;618(7965):467–79. https://doi.org/10.1038/s41586-023-05968-y

[12] Daniel AGS, Hacker CD, Lee JJ, et al. Homotopic functional connectivity disruptions in glioma patients are associated with tumor malignancy and overall survival. Neuro-Oncology Adv. 2021;3(1):1–10. https://doi.org/10.1093/noajnl/vdab176

[13] Louis DN, Perry A, Reifenberger G, et al. The 2016 World Health Organization Classification of Tumors of the Central Nervous System: a summary. Acta Neuropathol. 2016;131(6):803–20. https://doi.org/10.1007/s00401-016-1545-1

[14] Goyal MS, Blazey T, Metcalf N V., et al. Brain aerobic glycolysis and resilience in Alzheimer disease. Proc Natl Acad Sci U S A. 2023;120(7):1–8. https://doi.org/10.1073/pnas.2212256120

[15] Hammers A, Allom R, Koepp MJ, et al. Three-dimensional maximum probability atlas of the human brain, with particular reference to the temporal lobe. Hum Brain Mapp. 2003;19(4):224–47. https://doi.org/10.1002/hbm.10123

[16] Yan X, Kong R, Xue A, et al. Homotopic local-global parcellation of the human cerebral cortex from resting-state functional connectivity. Neuroimage. 2023;273(October 2022):120010. https://doi.org/10.1016/j.neuroimage.2023.120010

[17] Avants BB, Tustison NJ, Song G, et al. A reproducible evaluation of ANTs similarity metric performance in brain image registration. Neuroimage. 2011;54(3):2033–44.

http://dx.doi.org/10.1016/j.neuroimage.2010.09.025

[18] Silvestri E, Moretto M, Facchini S, et al. Widespread cortical functional disconnection in gliomas: an individual network mapping approach. Brain Commun. 2022;4(2):1–14. https://doi.org/10.1093/braincomms/fcac082

[19] Andersen SM, Rapcsak SZ, Beeson PM. Cost function masking during normalization of brains with focal lesions: Still a necessity? Neuroimage. 2010;53(1):78–84. http://dx.doi.org/10.1016/j.neuroimage.2010.06.003

[20] Feng X, Deistung A, Dwyer MG, et al. An improved FSL-FIRST pipeline for subcortical gray matter segmentation to study abnormal brain anatomy using quantitative susceptibility mapping (QSM). Magn Reson Imaging. 2017 Jun 1;39:110–22. https://doi.org/10.1016/j.mri.2017.02.002

[21] Deng S, Franklin CG, O'Boyle M, et al. Hemodynamic and metabolic correspondence of resting-state voxel-based physiological metrics in healthy adults. Neuroimage. 2022;250(January):118923. https://doi.org/10.1016/j.neuroimage.2022.118923

[22] Nugent S, Croteau E, Potvin O, et al. Selection of the optimal intensity normalization region for FDG-PET studies of normal aging and Alzheimer's disease. Sci Rep. 2020;10(1):1–8. http://dx.doi.org/10.1038/s41598-020-65957-3

[23] Miller KD, Ostrom QT, Kruchko C, et al. Brain and other central nervous system tumor statistics, 2021. CA Cancer J Clin. 2021;71(5):381–406. https://doi.org/10.3322/caac.21693

[24] Daniel AGS, Park KY, Roland JL, et al. Functional connectivity within glioblastoma impacts overall survival. Neuro Oncol. 2021;23(3):412–21. https://doi.org/10.1093/neuonc/noaa189

[25] Horwitz B, Duara R, Rapoport SI. Intercorrelations of glucosemetabolic rates between brain regions: Application to healthy males in a state of reduced sensory input. J Cereb Blood Flow Metab. 1984;4(4):484–99. https://doi.org/10.1038/jcbfm.1984.73

[26] Feeney DM, Baron JC. Diaschisis. Stroke. 1986;17(5):817–30. https://doi.org/10.1161/01.STR.17.5.817

[27] Jung E, Alfonso J, Monyer H, et al. Neuronal signatures in cancer. Int J Cancer. 2020;147(12):3281–91. https://doi.org/10.1002/ijc.33138

[28] Lv K, Hu Y, Cao X, et al. Altered whole-brain functional network in patients with frontal low-grade gliomas: a resting-state functional MRI study. Neuroradiology. 2024;66(5):775–84. https://doi.org/10.1007/s00234-024-03300-7

[29] Lin ZX. Glioma-related edema: New insight into molecular mechanisms and their

clinical implications. Chin J Cancer. 2013;32(1):49–52. https://doi.org/10.5732/cjc.012.10242

[30] Karavasilis E, Christidi F, Velonakis G, et al. Ipsilateral and contralateral cerebro-cerebellar white matter connections: A diffusion tensor imaging study in healthy adults. J Neuroradiol. 2019;46(1):52–60. http://dx.doi.org/10.1016/j.neurad.2018.07.004

[31] Buckner RL, Krienen FM, Castellanos A, et al. The organization of the human cerebellum estimated by intrinsic functional connectivity. J Neurophysiol. 2011;106(5):2322–45. https://doi.org/10.1152/jn.00339.2011

[32] Nenning KH, Furtner J, Kiesel B, et al. Distributed changes of the functional connectome in patients with glioblastoma. Sci Rep. 2020;10(1):1–11. https://doi.org/10.1038/s41598-020-74726-1

[33] Baumann C, Tichy J, Schaefer JH, et al. Delay in diagnosing patients with right-sided glioblastoma induced by hemispheric-specific clinical presentation. J Neurooncol. 2020;146(1):63–9. https://doi.org/10.1007/s11060-019-03335-4